Fluctuation properties of the eigenfrequencies and scattering matrix of closed and open unidirectional graphs with chaotic wave dynamics

Jiongning Che,[1] Xiaodong Zhang,[1] Weihua Zhang,[1,2] Barbara Dietz,[1,2,*] and Guozhi Chai[3]

[1]*Lanzhou Center for Theoretical Physics and the Gansu Provincial Key Laboratory of Theoretical Physics, Lanzhou University, Lanzhou, Gansu 730000, China*

[2]*Center for Theoretical Physics of Complex Systems, Institute for Basic Science (IBS), Daejeon 34126, Korea*

[3]*School of Physical Science and Technology, and Key Laboratory for Magnetism and Magnetic Materials of MOE, Lanzhou University, Lanzhou, Gansu 730000, China*

(Received 14 April 2022; accepted 4 July 2022; published 25 July 2022)

We present experimental and numerical results for the fluctuation properties in the eigenfrequency spectra and of the scattering matrix of closed and open unidirectional quantum graphs, respectively. Unidirectional quantum graphs, that are composed of bonds connected by reflectionless vertices, were introduced by Akila and Gutkin [Akila and Gutkin, J. Phys. A: Math. Theor. **48**, 345101 (2015)]. The nearest-neighbor spacing distribution of their eigenvalues was shown to comply with random-matrix theory predictions for typical chaotic systems with completely violated time-reversal invariance. The occurrence of short periodic orbits confined to a fraction of the system, that lead in conventional quantum graphs to deviations of the long-range spectral correlations from the behavior expected for typical chaotic systems, is suppressed in unidirectional ones. Therefore, we pose the question whether such graphs may serve as a more appropriate model for closed and open chaotic systems with violated time-reversal invariance than conventional ones. We compare the fluctuation properties of their eigenvalues and scattering matrix elements and observe especially in the long-range correlations larger deviations from random-matrix theory predictions for the unidirectional graphs. These are attributed to a loss of complexity of the underlying dynamic, induced by the unidirectionality.

DOI: 10.1103/PhysRevE.106.014211

I. INTRODUCTION

Quantum graphs [1–7], originally introduced by Pauling to model organic molecules [8], serve as a model for a large variety of systems, a few examples being quantum wires [9,10], optical waveguides [11], and mesoscopic quantum systems [12,13]. They consist of networks of bonds that are connected at vertices. The propagation of waves along the bonds of a quantum graph is governed by the one-dimensional Schrödinger equation and thus simple. Nevertheless, closed quantum graphs with incommensurable bond lengths behave like typical systems with chaotic classical dynamic. The complexity of their wave dynamics is determined by the incommensurability of the bond lengths and by the boundary conditions imposed on the wave functions entering and exiting a vertex. These are expressed in terms of unitary vertex matrices [2,6,10,14,15]. The ergodic dynamic results from the interference of the waves entering and exiting a vertex through the various bonds connected to it. Indeed, in Ref. [16] it is proven rigorously that the fluctuation properties in their eigenvalue spectra are described by the Gaussian ensembles of random-matrix theory (RMT) [17], in accordance with the Bohigas-Gianonni-Schmit (BGS) conjecture [18–21]. Moreover, the trace formula obtained in the semiclassical limit for their spectral density, which is given in terms of a sum over the associated periodic orbits, is exact [22]. Also the two-point correlation functions of the scattering (S) matrix describing chaotic scattering on the corresponding open graphs, obtained by coupling a graph to its environment through leads, i.e., bonds that extend to infinity, were shown to coincide with the corresponding RMT results [23–27].

The manifestation of characteristics of a classical dynamic in the spectral properties of the corresponding quantum system, like nuclei, atoms, molecules, quantum wires, and dots or other complex systems [28–36], is well understood and has been demonstrated, e.g., in numerous theoretical, numerical, and experimental studies based on billiard systems. The experimental modeling of quantum billiards [4,20,37,38] is performed with flat microwave resonators [39–45] and relies on the equivalence of the associated wave equations. Similarly, quantum graphs with Neumann or, generally, δ-type boundary conditions at the vertices [1–3,5] may be simulated with microwave networks [46] composed of coaxial cables coupled by joints at the vertices. These are wave dynamical systems; however, the BGS conjecture also applies to wave-chaotic systems [38,47]. It has been confirmed numerically already in Ref. [2] and experimentally in Refs. [46,48,49] that the fluctuation properties in the spectra of quantum graphs with preserved time-reversal ($\mathcal{T}$) invariance, that is, invariance with respect to an antiunitary operator $\hat{\boldsymbol{T}}$ with $\hat{\boldsymbol{T}}^2 = 1$, and with violated $\mathcal{T}$ invariance coincide with those of random matrices from the Gaussian orthogonal ensemble (GOE) and the Gaussian unitary ensemble (GUE), respectively. In the following we refer to these quantum graphs and microwave networks

*dietz@lzu.edu.cn

as conventional GOE and GUE graphs, respectively. Another advantage of microwave networks is that they can be employed to model experimentally quantum systems that are invariant with respect to the antiunitary operator where $\hat{\boldsymbol{T}}^2 = -1$ [50–54], whose spectral fluctuations were shown to coincide with those of random matrices from the Gaussian symplectic ensemble (GSE). The properties of open quantum graphs with wave chaotic dynamics have been investigated in [55–59].

Yet, there exist time-reversal-invariant quantum systems, with chaotic classical counterpart, whose spectral properties do not comply with those predicted by the BGS conjecture; that is, they do not coincide with those of random matrices from the GOE, but exhibit GUE statistics instead. A prominent example involves quantum billiards whose shapes possess a discrete rotational symmetry [60–64]. The universality class may be effected in the same way by certain dynamical properties, like unidirectionality of the classical dynamics which leads to a separation of the phase space into two ergodic components corresponding to the two distinct directions of propagation. Examples for billiards with this unidirectionality property are the constant-width and Monza billiards whose shapes can be designed such that the classical dynamics is fully chaotic [65–68]. In both cases the spectral properties coincide with GUE after extraction of a one-dimensional family of marginally stable bouncing-ball orbits that bounce back and forth perpendicularly between two opposite parts of the boundary.

In Ref. [69] unidirectional quantum graphs constructed from reflectionless vertices [14] are introduced, in which wave propagation is only allowed either in one direction or the opposite one. The nearest-neighbor spacing distribution of the eigenvalues of such quantum graphs and of nearly unidirectional ones is shown to coincide with that of random matrices from the GUE if the bond lengths are incommensurable. We investigate experimentally and also numerically to what extent the properties of closed unidirectional quantum graphs comply with GUE predictions and whether open ones may serve as models for quantum chaotic scattering systems with violated $\mathcal{T}$ invariance.

These studies are motivated by the aim to construct perfect quantum graphs exhibiting the fluctuation properties of random matrices from the GUE. Indeed, conventional quantum graphs have the drawback that they exhibit nongeneric features, originating from the backscattering at the vertices that leads to a confinement of waves propagating through the graphs to individual bonds or to a fraction of the graph [2,70,71] and thus to a nonergodic contribution to the dynamics. Their presence induces deviations from RMT predictions, since they do not experience the complexity of the underlying wave dynamics, which results from the scattering into the bonds attached to the vertices. Note that in the proof of the equivalence of the spectral properties of quantum graphs and of random matrices of the Gaussian ensembles provided in Refs. [16,24–26] such eigenstates were excluded.

Modes which are localized on individual bonds or a fraction of a quantum graph are nonuniversal in the sense that the associated eigenenergies depend on the lengths of the associated bonds [53]. Their effect on the spectral properties is, e.g., comparable to that of bouncing-ball orbits in a stadium billiard [72]. However, they comply with the particular boundary conditions at the vertices obeyed by the waves in conventional microwave networks and are thus unavoidable there. Since backscattering is suppressed in unidirectional quantum graphs, these nonuniversal effects are expected to be absent in them. Unidirectionality is achieved by an appropriate choice of the boundary conditions at the vertices or, equivalently, by the definition of the unitary matrices controlling the propagation of the waves across the vertices [14]. Namely, waves may enter a vertex only through part of the attached bonds and exit through the remaining ones and backward propagation is prohibited [69]. We would like to stress that there are other possible constructions for quantum graphs consisting of reflectionless bonds or exhibiting GUE statistics [6,14]; however, these either generate a simple wave dynamics or are not realizable experimentally.

Conventional microwave networks modeling GUE quantum graphs are obtained by introducing a directionality at one of the vertices [48,49], allowing waves to enter a vertex through all attached bonds, however, to exit through, respectively, one of them [73]. Thus, despite the presence of one directional vertex, waves may propagate in both directions on their bonds, in distinction to unidirectional graphs. Note that when constructing a microwave network exclusively from such directional vertices the number of possible paths for wave propagation will be drastically reduced so that in the worst case its spectrum consists of just one or a small number of fundamental eigenfrequencies and their overtones [74].

In a unidirectional quantum graph all vertices are required to possess the unidirectionality property, whereas in a conventional GUE network only one of the vertices needs to exhibit directionality. For an understanding of the effect of the complexity of the wave dynamics on the spectral properties we increased the number of directional vertices while keeping the total number of vertices fixed, thereby decreasing the number of itineraries along which waves may propagate through the graph. This feature is reflected in their length spectra, which are obtained from the Fourier transform of the spectral density from wavenumber to length [2,71] and exhibit peaks at the lengths of periodic orbits.

Deviations in the spectral properties caused by nonuniversal contributions, like by the shortest periodic orbits [72,75], become in particular visible in the long-range spectral fluctuation properties. We investigate them in terms of the number variance and the spectral rigidity [17] deduced from the two-point cluster function and the power spectrum [76–78], which is given in terms of the spectral form factor, i.e., the Fourier transform of the two-level cluster function [17]. In order to ensure that the deviations observed for the fluctuation properties in the experimental eigenfrequency spectra are intrinsic and not due to the fact that the frequency range, where the analogy between the Helmholtz equation of the coaxial cables and the one-dimensional Schrödinger equation holds, comprises only a few hundreds of eigenfrequencies, we, in addition, performed numerical simulations using several thousands of eigenvalues of the corresponding quantum graphs.

We briefly introduce in Sec. II quantum graphs, microwave networks, and the scattering formalism used to describe the fluctuation properties of the S matrix associated with their open counterparts. In Sec. III we present results for the spec-

tral properties of unidirectional quantum graphs and compare them to those of GUE quantum graphs and graphs containing directional vertices and in Sec. IV those of the S matrix associated with the measurement process. Finally, our findings are discussed in Sec. V.

II. CONVENTIONAL, PARTLY DIRECTIONAL, AND UNIDIRECTIONAL QUANTUM GRAPHS AND MICROWAVE NETWORKS

A quantum graph consists of $\mathcal{V}$ vertices $i = 1, \ldots, \mathcal{V}$ that are connected by $\mathcal{B}$ bonds. It is characterized by the connectivity matrix $\hat{C}$ with diagonal elements $C_{ii} = 0$ and off-diagonal elements $|C_{ij}| = 1$ if vertices i and j are connected and $C_{ij} = 0$ otherwise, and the lengths of the bonds denoted by L_{ij}. The wave function components $\psi_{ij}(x)$ on these bonds are solutions of the one-dimensional Schrödinger equation

$$\frac{d^2}{dx^2}\psi_{ij}(x) + k^2\psi_{ij}(x) = 0, \tag{1}$$

where the coordinate x varies along the bond from $x = 0$ at vertex i to $x = L_{ij}$ at vertex j. They are subject to boundary conditions imposed at vertices i and j that ensure continuity,

$$\psi_{ij}(x = 0) = \varphi_i, \quad \psi_{ij}(x = L_{ij}) = \varphi_j, \quad i < j, \tag{2}$$

that is, at the vertices i all wave functions entering or exiting from it have to take the same value φ_i. A further boundary condition results from the requirement that for closed quantum graphs at each vertex the current should be conserved. We restrict here to Kirchhoff boundary conditions, which can be modeled experimentally. They constitute a special case of δ-type boundary conditions [2,4,5,10],

$$-\sum_{j<i} C_{ji}\frac{d}{dx}\psi_{ji}(x = L_{ij}) + \sum_{j>i} C_{ij}\frac{d}{dx}\psi_{ij}(x = 0) = \lambda_i\varphi_i. \tag{3}$$

Based on these boundary conditions at each vertex i a unitary matrix $\hat{\sigma}^{(i)}_{ji,im}$ with dimension given by its valency v_i can be defined, which reflects the continuation of a wave function entering it from the vertex m and proceeding towards vertex j,

$$\sigma^{(i)}_{ji,im} = \left(-\delta_{j,m} + \frac{1}{v_i}\left[1 + \frac{1 - i\Lambda_i}{\sqrt{1 + \Lambda_i^2}}\right]\right)C_{ij}C_{im},$$
$$\Lambda_i = \frac{\lambda_i}{v_i k}. \tag{4}$$

The eigenwavenumbers of a quantum graph with these boundary conditions are determined by solving the equation [2]

$$\det \hat{h}(k) = 0, \tag{5}$$

with

$$h_{ij}(k) = \begin{cases} -\sum_{m\neq i}\cos(kL_{im})\frac{C_{im}}{\sin(kL_{im})} - \frac{\lambda_i}{k}, & i = j \\ \frac{C_{ij}}{\sin(kL_{ij})}, & i \neq j. \end{cases} \tag{6}$$

The components of the associated eigenvectors yield the values of the wave functions at the vertices i, φ_i, and thus the eigenfunctions [2]. The case $\lambda_i = 0$, which corresponds to Neumann boundary conditions, can be modeled with microwave networks [46]. It has been shown in Refs. [16,26] that for this case, and generally, for finite values of the λ_i a quantum graph exhibits spectral properties of a typical wave-chaotic system, if the bond lengths are incommensurable. To realize a quantum graph with induced $\mathcal{T}$ invariance, a magnetic field is introduced at part or all of the bonds, yielding for the Schrödinger equation

$$\left(-i\frac{d}{dx} - A_{ij}\right)^2\psi_{ij}(x) + k^2\psi_{ij}(x) = 0, \tag{7}$$

with $A_{ij} = -A_{ji}$ denoting the corresponding magnetic vector potential. In the numerical simulations we choose $A_{ij} = \pi/2$. The eigenvalue equation of such a graph is obtained from Eq. (6) by multiplying the corresponding matrix elements h_{ij} with a phase factor $e^{-iA_{ij}L_{ij}}$ [2].

Our main objects of interest are quantum graphs and microwave networks that contain vertices inducing a certain directionality. For their construction we do not specify boundary conditions. Instead we introduce a unitary matrix $\hat{U}^{(i)}$, which defines the propagation of waves through the vertex i and imposes local vertex conditions which ensure self-adjointness, that is, continuity and conservation of the current. To determine the vertex scattering matrix which meets these requirements, we proceed as in Ref. [7], yielding

$$\hat{\sigma}^{(i)} = [\hat{U}^{(i)} - \kappa\,\mathbb{1}]^{-1}[\mathbb{1} - \kappa\hat{U}^{(i)}] \tag{8}$$

with

$$\kappa = \frac{1 - k}{1 + k}. \tag{9}$$

The microwave networks are constructed from coaxial microwave cables (HASCO SMA-RG402) that are coupled by joints that correspond to the vertices. For all quantum graph and network designs considered in the present article the valency of the vertices is four. To realize quantum graphs with preserved $\mathcal{T}$ invariance, we used homemade joints [79]. The corresponding scattering matrix depends on frequency, however, is well approximated by a *type A joint*:

$$\hat{S}^J = \frac{1}{2}\begin{pmatrix} -1 & 1 & 1 & 1 \\ 1 & -1 & 1 & 1 \\ 1 & 1 & -1 & 1 \\ 1 & 1 & 1 & -1 \end{pmatrix}. \tag{10}$$

Replacing in Eq. (8) $\hat{U}$ by $\hat{S}^J$ yields for the vertex matrix $\hat{\sigma}^J$ of the corresponding quantum graph that for Neumann boundary conditions given in Eq. (4) [46], i.e., $\hat{\sigma}^J = \hat{S}^J$.

A coaxial cable consists of an inner and a concentric outer conductor and the space between them is filled homogeneously with Teflon with an experimentally determined dielectric constant $\epsilon \simeq 2.06$. Below the cutoff frequency for the first transverse electric (TE_{11}) mode only the fundamental transverse electromagnetic (TEM) mode can propagate between the conductors [80,81]. The one-dimensional telegraph equation of these Lecher waves propagating between the inner and outer conductors along such a coaxial cable is given in terms of the difference $V_{ij}(x)$ between the potentials at the conductors' surfaces,

$$\frac{d^2}{dx^2}V_{ij}(x) + \frac{\omega^2\epsilon}{c^2}V_{ij}(x) = 0, \quad i < j. \tag{11}$$

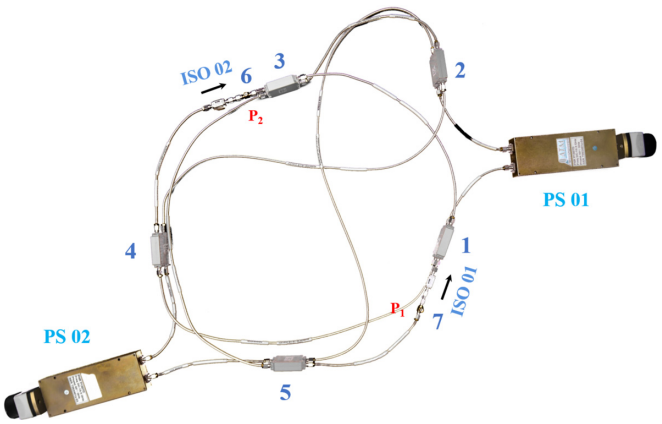

FIG. 1. Photograph of the microwave network simulating the quantum graph shown in Fig. 2. Microwave power is coupled in and out at the antenna ports P1 and P2 marked by 6 and 7 that are coupled to the vector network analyzer. Unidirectionality is achieved with hybrids. Furthermore, isolators ISO 01 and ISO 02 are introduced at the ports, to ensure unidirectionality of the microwaves coupled in and out of the microwave network. To attain an ensemble of unidirectional quantum graphs the lengths of two bonds are changed by using phasers PS 01 and PS 02. Here, the length of one bond is increased and that of another one is decreased by the same amount, to keep the spectral density unchanged.

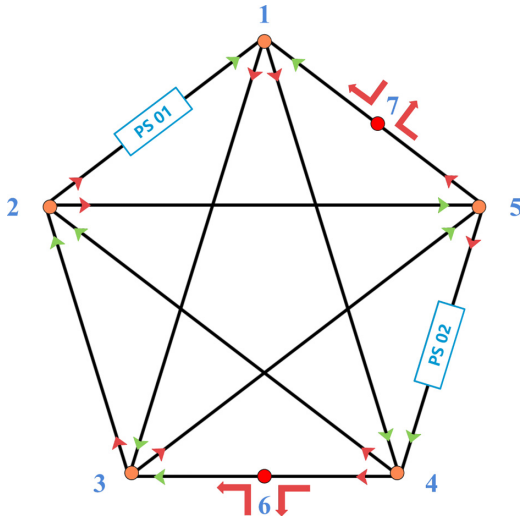

FIG. 2. Schematic view of the unidirectional quantum graph. The direction of wave propagation at each vertex is indicated by arrows. An ensemble of such graphs is realized by increasing the length of one bond and decreasing it at another one by the same amount (marked by PS 01 and PS 02). The quantum graph is attached to leads at the vertices marked by 6 and 7.

Here, ϵ is the dielectric constant of the medium, $\omega = 2\pi f$ is the angular frequency with f the microwave frequency, and c is the velocity of light. Equation (11) is exact for lossless coaxial cables, that is, for vanishing Ohmic resistance. At the vertices $V_{ij}(x)$ obeys the continuity equation and for conventional joints Eq. (3) with $\lambda_i = 0$. Thus, below the cutoff frequency the wave equations (11) governing the $V_{ij}(x)$ are mathematically identical to the Schrödinger equation (1) of a quantum graph with Neumann boundary condition at the vertices [2,4] when identifying $\sqrt{\epsilon}\frac{\omega}{c}$ of the microwave network with the wavenumber k of the quantum graph. Hence the eigenfrequencies f_i of a microwave network yield the eigenwavenumbers $k_i = \frac{2\pi f_i}{c}$ of the quantum graph of corresponding geometry whose bond lengths are obtained by multiplying those of the coaxial cables by $\sqrt{\epsilon}$ yielding their optical lengths. The eigenfrequencies of a microwave network are determined experimentally by attaching antennas to ports marked by 6 and 7 in Fig. 1, which are coupled to a vector network analyzer (Keysight N5227A), and measuring the transmission and reflection amplitudes as function of the microwave frequency f [53]. The microwave networks are slightly opened through the antennas. Therefore, we employed in addition to the secular equation (6) the scattering formalism for open quantum graphs [4,6,82] for the quantization of the quantum graphs, which is more appropriate for the description of the experimental situation. The quantum graph is converted into a scattering system by attaching leads to it at vertices 6 and 7 in Fig. 2 that extend to infinity. These are modeled by the antenna ports in the corresponding microwave network. The S matrix describing the scattering process of the waves entering the graph through these leads from infinity and exiting from it through the same (reflection) or the other lead (transmission) is accounted for by a $(2\mathcal{B} \times 2\mathcal{B})$-dimensional bond S matrix $\hat{S}_{\mathcal{B}}(k)$ [4,82], where $\mathcal{B}$ denotes the number of bonds. Within this scattering approach the eigenvalues of the closed quantum graph are given by the solutions of the secular equation [2]

$$\zeta_{\mathcal{B}}(k) = \det[\mathbb{1} - \hat{S}_{\mathcal{B}}(k)] = 0, \tag{12}$$

where

$$\hat{S}_{\mathcal{B}}(k) = \hat{D}(k)\hat{T} \tag{13}$$

in the $2\mathcal{B}$ space of directed bonds, and

$$\hat{D}_{ij,nm} = \delta_{i,n}\delta_{j,m}e^{ikL_{ij}}, \tag{14}$$

$$\hat{T}_{ji,nm} = \delta_{n,i}C_{j,i}C_{n,m}\hat{\sigma}^{(i)}_{ji,nm}. \tag{15}$$

Applying the expansion

$$\ln\det[\mathbb{1} - \hat{S}_{\mathcal{B}}(k)] = -\sum_{p=1}^{\infty}\frac{1}{p}\mathrm{tr}\hat{S}^{p}_{\mathcal{B}}(k) \tag{16}$$

yields that $\ln\zeta_{\mathcal{B}}(k)$ equals a sum over terms whose phases equal kl_p, with $l_p = \sum_{n=1}^{p} L_{i_n i_{n+1}}$, $i_n \in \{1, 2, \ldots, \mathcal{V}\}$, $i_{p+1} = i_1$ denoting the lengths of the possible loops along p successive connected vertices through the graph [2], implying that the secular equation provides a direct link between the spectral properties of a quantum graph and the complexity of its dynamics [6]. Indeed, starting from the secular equation (12), an exact trace formula has been derived in Ref. [2] for the spectral density of quantum graphs constructed from vertices with δ-type boundary conditions (3),

$$\rho^{\mathrm{fluc}}(k) = \frac{1}{\pi}\sum_{p\in\mathcal{P}_n}\frac{l_p\cos\left(r[kl_p + \pi\mu_p]\right)}{e^{r(n_p\gamma_p/2)}} \tag{17}$$

with

$$e^{-n_p\gamma_p/2} = \prod_{s=1}^{\mu_p}\left|\left(1 - \frac{2}{v_s}\right)\right|\prod_{s=1}^{n_p-\mu_p}\left|\frac{2}{v_s}\right|. \tag{18}$$

The sum is over periodic orbits, that emerge from a repeated looping of the primitive periodic orbits $p \in \mathcal{P}_n$ consisting of n_p vertices, with $n = rn_p$ denoting the period after r repetitions. The lengths l_p of the primitive periodic orbits are given by the sum over the lengths of the bonds that connect its n_p vertices and μ_p denotes the number of vertices with $v_i \geqslant 2$, where backscattering occurs. In Ref. [6] trace formulas are derived beyond the orthogonal and unitary symmetry class and universality of the spectral properties and thus applicability of RMT is proven based on the semiclassical and supersymmetry approach for incommensurable quantum graphs. Agreement of the spectral properties of such quantum graphs with RMT predictions originates from the ergodicity of the phases of the matrix in Eq. (14) that constitute those in the trace formula of the spectral density and spectral functions like, e.g., the two-point correlation function, deduced from it. We will provide examples, where phase ergodicity is destroyed and we ascribe deviations from RMT predictions to this, as outlined below.

We performed experiments with the unidirectional microwave network shown in Fig. 1 and numerical computations for the corresponding quantum graph shown in Fig. 2 and also with variants of them, obtained by using joints that do not have the directionality property indicated in Fig. 2. The valency of all joints in Figs. 1 and 2 equals four, except for the vertices where the antennas (respectively leads) are attached. We realize a conventional microwave network modeling the spectral properties and scattering properties of a quantum graph with violated $\mathcal{T}$ invariance by replacing in the corresponding GOE network one of the type A joints in Eq. (10) by two coupled circulators (Pasternack PE8403). As illustrated in Fig. 3, the transmission and reflection spectra of a coupled circulator are well described by a *type B joint*,

$$\hat{S}^C = \begin{pmatrix} 0 & 0 & 0 & 1 \\ 1 & 0 & 0 & 0 \\ 0 & 1 & 0 & 0 \\ 0 & 0 & 1 & 0 \end{pmatrix}, \tag{19}$$

in a finite frequency range $7 \lesssim f \lesssim 14$ GHz. The vertex scattering matrix of the corresponding quantum graph is obtained by replacing $\hat{U}$ in Eq. (8) by $\hat{S}^C$, yielding

$$\hat{\sigma}^C = \begin{pmatrix} -\kappa & \kappa^2 & \kappa & 1 \\ 1 & -\kappa & \kappa^2 & \kappa \\ \kappa & 1 & -\kappa & \kappa^2 \\ \kappa^2 & \kappa & 1 & -\kappa \end{pmatrix}. \tag{20}$$

Thus, the vertex matrix of the corresponding quantum graph depends on k, and approximates the scattering matrix of the microwave network well only for values of k close to one, where k can be rescaled according to the experimental conditions. Yet, it has been shown experimentally [48] that a microwave network containing a circulator serves as a good model for quantum graphs in which $\mathcal{T}$-invariance violation is induced by introducing a magnetic field in the bonds corresponding to the coaxial cables that are attached to the circulator [see Eq. (7)]. Accordingly, we performed numerical computations with such quantum graphs and compared them with the experimental results for the GUE microwave networks with one type B joint. For the realization of the unidirectional graph shown in Fig. 2 we use hybrids (Pasternack PE2CP11602052). As shown in Fig. 4 they are well described

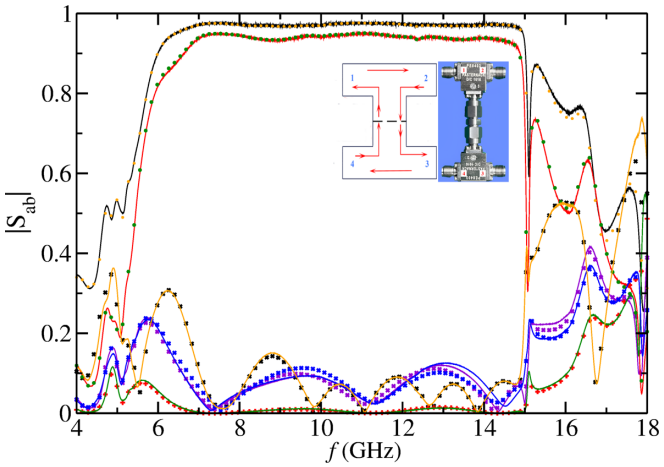

FIG. 3. Transmission spectra $|S_{ab}|$ of the coupled circulators for $b = 1, a = 2$ and $b = 2, a = 1$ (black line and crosses), $b = 2, a = 3$ and $b = 3, a = 2$ (green dots and line), $b = 3, a = 4$ and $b = 4, a = 3$ (orange dots and line), $b = 4, a = 1$ and $b = 1, a = 4$ (red line and dots), $b = 1, a = 3, b = 3, a = 1$ (violet crosses and line) and $b = 2, a = 4$ and $b = 4, a = 2$ (blue line and crosses). Since reflection is suppressed at all vertices, the spectra $|S_{aa}|$ are not shown. Thus, in the frequency range [7,15] GHz the transmission and reflection properties of the coupled circulators are well described by the scattering matrix Eq. (19).

by the scattering matrix (*type C joint*)

$$\hat{S}^H = \frac{1}{\sqrt{2}} \begin{pmatrix} 0 & 0 & 1 & 1 \\ 0 & 0 & -1 & 1 \\ 1 & -1 & 0 & 0 \\ 1 & 1 & 0 & 0 \end{pmatrix}. \tag{21}$$

The vertex scattering matrix of the corresponding quantum graph coincides with this scattering matrix; i.e., $\hat{\sigma}^H = \hat{S}^H$.

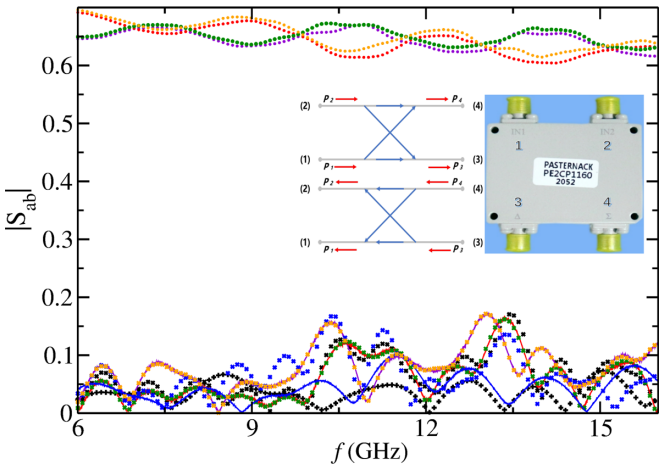

FIG. 4. Transmission and reflection spectra $|S_{ab}|$ and $|S_{aa}|$ of the hybrid for $a = 1, b = 2$ (black crosses and plus), $a = 2, b = 3$ (red dots and line), $a = 3, b = 4$ (blue crosses and line), $a = 4, b = 1$ and $a = 1, b = 4$ (red dots and line), $a = 1, b = 3$ (violet dots and line), and $a = 2, b = 4$ (green dots and crosses). Since $|S_{ab}| = |S_{ba}|$ and $|S_{aa}| \simeq |S_{bb}|$ not all spectra are shown. Thus, the transmission and reflection properties of the hybrids are well captured by the vertex matrix in Eq. (21).

Thus, the wave equations of microwave networks with hybrids as joints coincide with that of the quantum graph with corresponding geometry and vertex matrix given in Eq. (21).

The bond S matrix of the microwave network depicted in Fig. 1 without the isolators ISO 01 and ISO 02, or the quantum graph shown schematically in Fig. 2, can be brought to a block-diagonal form [69]

$$\hat{S}_{\mathcal{B}}(k) = \begin{pmatrix} \hat{S}^{+}_{\mathcal{B}}(k) & \hat{0} \\ \hat{0} & \hat{S}^{-}_{\mathcal{B}}(k) \end{pmatrix}, \tag{22}$$

where each block matrix accounts for one direction of flow. The solutions of Eq. (12) coincide for $\hat{S}^{\pm}_{\mathcal{B}}(k)$; that is, the eigenvalues of a unidirectional graph allowing both directions of flow are pairwise degenerate.

The total optical length of the coaxial cables used in all experiments and the geometric lengths of the bonds in the corresponding quantum graphs equaled $\mathcal{L} \simeq 4.418$ m. However, the optical lengths of the conventional joints, coupled circulators, and hybrids differ considerably from each other. Accordingly, the total optical lengths of the microwave networks and thus the average spectral density $\bar{\rho}(k)$, which is given by Weyl's formula,

$$\bar{\rho}(f) = \frac{2\mathcal{L}}{c}, \tag{23}$$

changes when replacing a joint by one with differing transmission properties. In the numerical simulations we accounted for these changes of the bond lengths.

An ensemble of quantum graphs and microwave networks was realized as in Refs. [49,53] by varying the lengths of two bonds in $N_{\max} = 50$ steps by an increment $\Delta l = 0.83$ mm. In the microwave networks this is done with two phase shifters (ATM P1507D), denoted by PS 01 and PS 02 in Fig. 1. A phase shift $\Delta\varphi$ induces a k-dependent change $\Delta\tilde{l}$ of the length,

$$\Delta\varphi = k\Delta\tilde{l} = \frac{2\pi\nu}{c}\Delta\tilde{l}. \tag{24}$$

In order to keep the spectral density fixed, the length of one bond was increased and that of the other one was decreased by the same amount.

The measurement of spectra for an ensemble of graphs facilitates the identification of the eigenfrequencies f_i of the microwave networks. These correspond to the positions of the minima exhibited by the reflection amplitude $|S_{11}(f)|$ when measured as a function of the microwave frequency f. They are broadened because of the unavoidable absorption of microwaves in the coaxial cables and thus may overlap, which complicates the identification of eigenfrequencies. The problem of absorption can be circumvented in experiments with flat, cylindrical microwave resonators simulating quantum billiards [39,40,42,83] by using superconducting cavities [40,47,84]. This is not possible with microwave networks, because the coaxial cables contain Teflon. In the experiments with the GUE graphs about 6% of the number of levels predicted by Weyl's law were missing. As mentioned above, the eigenfrequencies of a unidirectional graph admitting both directions, that is, incoming waves at ports 1 and 2 or incoming waves at ports 3 and 4 of the hybrid shown in Fig. 4, are pairwise degenerate. In order to avoid these degeneracies, which hamper the identification of the eigenfrequencies, we added isolators (Ditom DMI6018), denoted by ISO 01 and ISO 02 in Fig. 1, to the ports marked by 6 and 7 so that the microwaves coupled in and out follow one direction of the unidirectional flow. Due to the halved resonance density, we were able to detect all eigenfrequencies in the frequency range [6,12] GHz. Here, we exploited the level dynamic [53].

Similarly, the fluctuation properties of the bond scattering matrix (13) are expected to comply with those of quantum chaotic scattering systems. It, indeed, is demonstrated in Refs. [24–26] that the correlation functions of the S-matrix elements of open quantum graphs coincide with the corresponding RMT results [23,27] for quantum chaotic scattering systems. Actually, the S matrix describing this scattering process can be brought to the form

$$\hat{S}_{\mathcal{V}}(k) = \mathbb{1} - 2\pi\hat{W}^{T}(\hat{h}(k) + i\pi\hat{W}\hat{W}^{T})^{-1}\hat{W}, \tag{25}$$

which is similar to that derived on the basis of the S-matrix formalism for compound nucleus reactions [85]. That S matrix, in fact, has been shown to be mathematically identical to that for microwave resonators [86]. This analogy has been employed in a sequence of experiments [87–92] to investigate universal properties of the S matrix for compound-nucleus reactions and, generally, for quantum scattering processes with intrinsic chaotic dynamics, that is, to verify analytical results derived on the basis of the supersymmetry and the RMT approach [91,93–95]. In Sec. IV we review our results on the fluctuation properties of the S matrix of the unidirectional graph shown in Fig. 2 and of the microwave network with the same geometry, but constructed from four type A and one type B joints, and compare them to those deduced from the RMT scattering approach. Furthermore, we reduced the complexity of the dynamics of the microwave network by replacing an increasing number of type A joints by type B joints.

III. SPECTRAL PROPERTIES OF UNIDIRECTIONAL MICROWAVE NETWORKS

We computed fluctuation properties in the eigenfrequency spectra of the unidirectional microwave network shown in Fig. 1 and of the corresponding unidirectional graph shown in Fig. 2, constructed from type C vertices with vertex matrix given in Eq. (21) and of the GUE microwave network of the same geometry, where the joint marked by 2 in Fig. 2 was replaced by a type B joint and the others by conventional type A ones with the scattering matrices given in Eqs. (10) and (19), respectively. For its numerical simulation we used a quantum graph with type A vertices, governed by the Schrödinger equation (7) along the bonds that are attached to the vertex marked by 2 in Fig. 2 and by Eq. (1) otherwise. The spectral properties were compared with RMT results for random matrices from the GUE. For this we removed system-specific properties by unfolding the eigenfrequencies f_n to mean spacing unity, $\epsilon_n = \bar{\rho} f_n$, where the average spectral density is given in Eq. (23).

We analyzed short-range correlations in the eigenvalue spectra of the quantum graphs and microwave networks in terms of the nearest-neighbor spacing distribution $P(s)$ of adjacent spacings $s_i = \epsilon_{i+1} - \epsilon_i$ and its cumulant $I(s) = \int_0^s ds' P(s')$, which has the advantage that it does not depend on the binning size of the histograms yielding $P(s)$. Another

measure for short-range correlations is the distribution of the ratios [96,97] of consecutive spacings between next-nearest neighbors, $r_j = \frac{\epsilon_{j+1}-\epsilon_j}{\epsilon_j-\epsilon_{j-1}}$. Ratios are dimensionless so the nonunfolded eigenvalues can be used [96–98]. Furthermore, we considered the variance $\Sigma^2(L) = \langle (N(L) - \langle N(L)\rangle)^2\rangle$ of the number of unfolded eigenvalues $N(L)$ in an interval of length L, and the rigidity $\Delta_3(L) = \langle \min_{a,b} \int_{e-L/2}^{e+L/2} de[N(e) - a - be]^2\rangle$ as measures for long-range correlations. Here, $\langle\cdot\rangle$ denotes the average over an ensemble of random matrices or of microwave-network or quantum-graph realizations. Furthermore, we analyzed the power spectrum which is given in terms of the Fourier transform of the deviation of the qth nearest-neighbor spacing from its mean value q, $\delta_q = \epsilon_{q+1} - \epsilon_1 - q$, from q to τ,

$$s(\tau) = \left\langle \left| \frac{1}{\sqrt{N}} \sum_{q=0}^{N-1} \delta_q \exp\left(-2\pi i \tau q\right) \right|^2 \right\rangle, \tag{26}$$

for a sequence of N levels, where $0 \leqslant \tau \leqslant 1$. It exhibits for $\tau \ll 1$ a power law dependence $\langle s(\tau)\rangle \propto \tau^{-\alpha}$ [76,77], where for regular systems $\alpha = 2$ and for chaotic ones $\alpha = 1$ independently of whether $\mathcal{T}$ invariance is preserved or not [34,99–103]. It was studied experimentally for microwave networks with preserved and violated $\mathcal{T}$ invariance and with symplectic symmetry [49,54].

In Fig. 5 we compare the spectral properties of the unidirectional microwave networks (top), obtained from 50 sequences of 136 eigenfrequencies (red solid lines), and of the GUE microwave network (bottom), obtained from 17 sequences consisting of 197 eigenfrequencies (red solid lines), with those of the unidirectional and GUE quantum graph (blue dashed lines), where we took into account up to 6500 eigenvalues to check the effect of the lengths of the spectra on the spectral properties. The numerical and experimental results agree well for the unidirectional graph, whereas for the GUE graph they agree well after extraction of 6% of the eigenvalues. The latter are compared to the analytical results for GUE sequences [49,104] with 6% missing levels (green dash-dotted lines), the former to the predictions for the GUE (black dash-dotted lines). For both cases the short-range correlations agree well with the corresponding RMT results. However, for the unidirectional graph, deviations from the GUE curves (black dash-dotted lines) are observed in the number variance already around $L \approx 1.5$ and for the rigidity around $L = 4$, whereas for the GUE graph, deviations from the GUE curve accounting for missing levels (green dash-dotted line) are observed around $L = 3$–4, and around $L = 9$ for the numerical results (blue dashed line) only, respectively. These deviations cannot result from too short sequences, because the numerical results show the same deviations as the experimental graphs. For a better understanding of their origin we computed 6500 eigenvalues for the GOE graph and graphs with varying number of joints described by the vertex matrix in Eq. (19) and by Eq. (10) otherwise, to simulate microwave networks of corresponding geometry. We would like to emphasize that these numerical simulations only provide an approximation for a quantum graph with the vertices described by the corresponding vertex scattering matrix in Eq. (20). Yet, our intention is not to give an exact theoretical description but to obtain insight into the effect of type B joints on the spectral properties of the microwave networks.

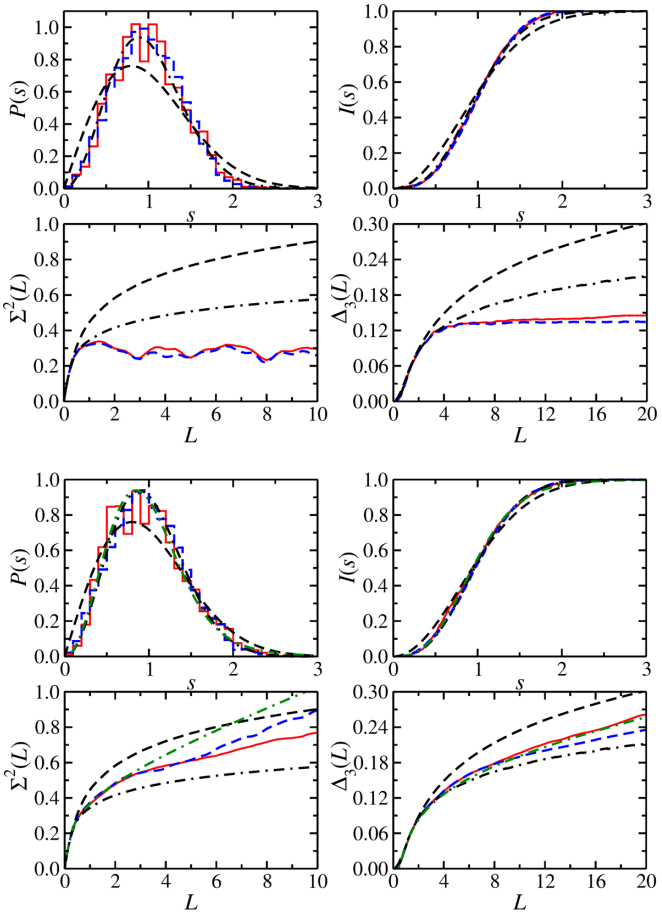

FIG. 5. Comparison of the spectral properties of the experimentally (red solid lines) and the numerically (blue dashed lines) obtained results for the unidirectional quantum graph (top), and for the microwave network constructed from one type A and conventional type B joints otherwise and the GUE quantum graph (bottom). The green dash-dotted lines in the latter show the analytical result for incomplete GUE spectra with 6% missing levels. The black dashed and dash-dotted lines exhibit the results for random matrices from the GOE and GUE, respectively.

In Fig. 6 we show the spectral properties for the GOE graph (orange solid lines), and for graphs with one (red), two (green), three (blue), and four (violet) type B joints described by Eq. (19) and by type A joints with Eq. (10), otherwise. Furthermore, we show again the numerical result for the unidirectional graph (turquoise histogram and circles). The largest deviations from the GUE results are observed for the latter. In the other cases the spectral properties approach those of the unidirectional one with increasing number of type B joints that introduce a directionality as illustrated in Fig. 3. Corresponding results for the power spectrum are shown in Figs. 7 and 8. Large deviations of the experimental and numerical results from the RMT prediction are observed for the unidirectional graph and for an increasing number of type B joints. The ratio distributions, which provide another measure for short-range correlations, are exhibited in Fig. 9. They agree well with the GUE results for the unidirectional and the GUE graphs.

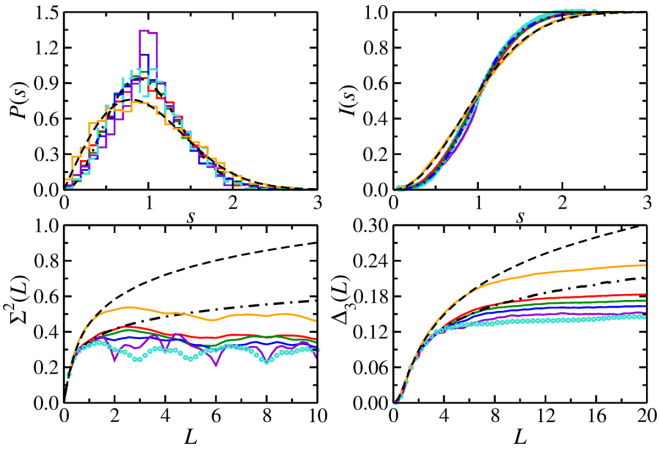

FIG. 6. Comparison of the spectral properties of 6500 numerically obtained eigenvalues of the nonunidirectional quantum graph (orange) with five conventional joints, graphs with one (red), two (green), three (blue), and four (violet) type *B* joints and conventional type *A* joints otherwise, and the unidirectional (turquoise) quantum graph with five type *C* joints, respectively. The black dashed and dash-dotted lines exhibit the results for random matrices from the GOE and GUE, respectively.

In summary, agreement with GUE predictions worsens with increasing number of type *B* joints characterized by the vertex matrix in Eq. (19), which induces a directionality and the spectral properties approach those of the unidirectional graph. This may be attributed to an increasing loss of complexity of the wave dynamics. Indeed, when replacing all joints in Fig. 2 by vertices governed by Eq. (19) there are only three itineraries along which waves may propagate through the network of bonds. Accordingly, the number of primitive periodic orbits contributing to the trace formula deduced from the secular equation (12) decreases with increasing number of type *B* joints, thus yielding a deprivation of ergodicity of the phases entering it and the two-point correlation function deduced from it, which yields the number variance and rigidity [6]. As a consequence the eigenfrequency spectrum is reduced to a small number of fundamental modes for four and five type *B* joints, as indicated by the dominant peak in the nearest-neighbor spacing distribution for four type *B* joints,

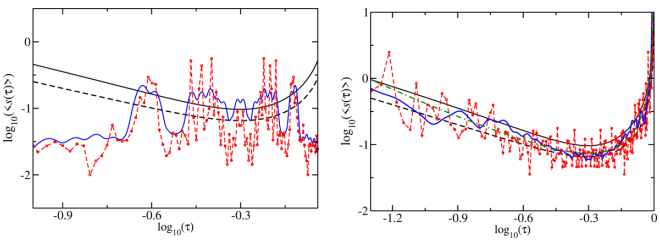

FIG. 7. Comparison of the power spectrum of the experimentally (red) and the numerically (blue) obtained results for the unidirectional (left) quantum graph, and the graph with one type *B* joint and GUE graph of corresponding geometry (right). The green dash-dotted line in the right part shows the analytical result for the incomplete GUE spectra with 6% missing levels. The black solid and dashed lines exhibit the results for random matrices from the GOE and GUE, respectively.

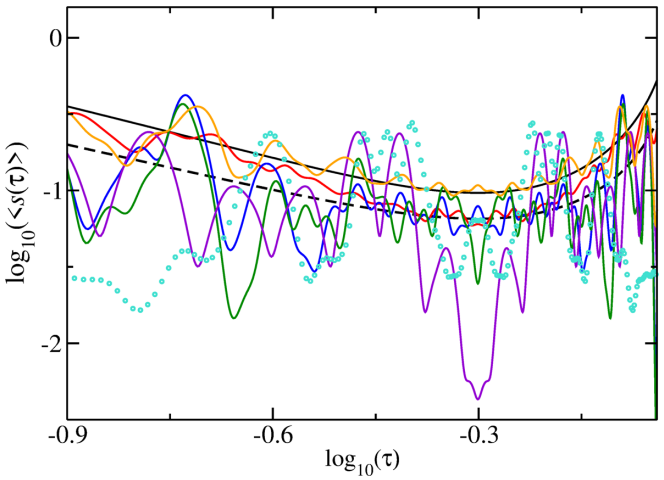

FIG. 8. Comparison of the power spectrum obtained from the 6500 numerically computed eigenvalues of the GOE graph (orange) with five conventional joints, graphs with one (red), two (green), three (blue), and four (violet) type *B* joints and conventional type *A* joints otherwise, and the unidirectional (turquoise) quantum graph with five type *C* joints, respectively. The black solid and dashed lines exhibit the results for random matrices from the GOE and GUE, respectively.

which implies that the spectrum contains a dominant sequence of equidistant eigenfrequencies.

To corroborate this conclusion we analyzed length spectra. The upper part of Fig. 10 shows the length spectrum obtained from the eigenfrequencies of the unidirectional microwave network (green solid lines) in comparison to that obtained from the first 400 eigenvalues of the corresponding quantum graph (red line) and of the GOE graph. The lower part shows the length spectra of the GOE and unidirectional graphs obtained for 6500 eigenvalues and the results deduced from the semiclassical trace formula in Eq. (17) for periodic orbits

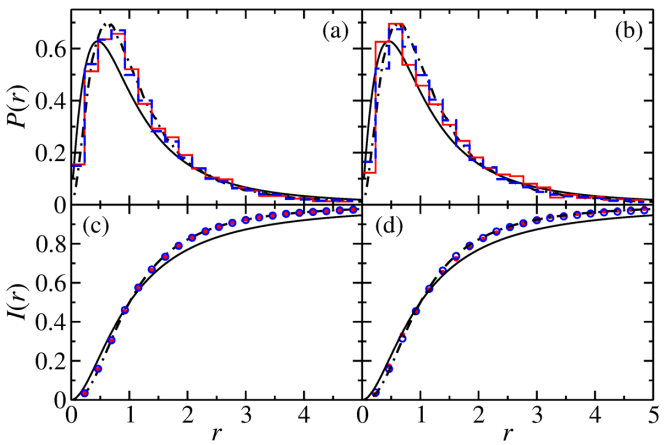

FIG. 9. Comparison of the ratio distributions (upper panels) and the cumulative ratio distributions (lower parts) of the experimentally (red) and the numerically (blue) obtained results for the unidirectional (left) and GUE (right) quantum graph. The black solid and dash-dotted lines exhibit the results for random matrices from the GOE and GUE, respectively.

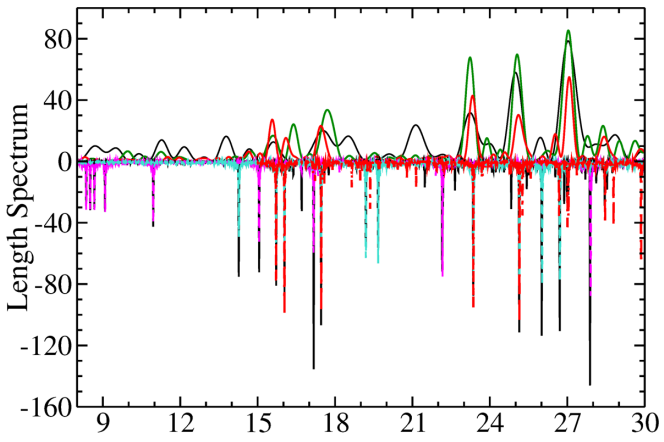

FIG. 10. Length spectra $\sigma|\tilde{\rho}(l)|$ obtained from the unfolded eigenfrequencies of the microwave network shown in Fig. 1 (green), the GOE quantum graph with conventional joints (black lines) and the unidirectional quantum graph (red solid and dashed lines) shown in Fig. 2, for 400 and 6500 numerically obtained eigenvalues with $\sigma = 1$ and $\sigma = -1$, respectively, in comparison to the length spectra with $\sigma = -1$ deduced from the trace formula for periodic orbits of period $n_p = 2$ (magenta dashed line) and $n_p = 3$ (turquoise dashed line), respectively.

bouncing back and forth on individual bonds with $n_p = 2$ (magenta dashed line) and of periodic orbits along loops consisting of $n_p = 3$ (turquoise dashed line) vertices. Comparing the length spectra shows that periodic orbits confined to a single bond are missing in the unidirectional graph and microwave network that are held responsible for the deviations from RMT predictions [71]. Therefore, we expected that agreement of the spectral properties of unidirectional graphs with the RMT predictions is better than for conventional graphs. However, due to the unidirectionality also some periodic orbits with larger n_p values may not occur, as illustrated for $n_p = 3$ in Fig. 10 implying a loss of complexity of the wave dynamics in the graph [14]. From our findings for the spectral properties we may conclude that unidirectional graphs may not generate a wave dynamics of sufficient complexity in the quantum graphs, in the sense that agreement with GUE statistics is only observed in the short-range correlations. Deviations of correlations between the eigenfrequencies or eigenvalues from GUE behavior are observed already at distances larger than a few mean spacings L.

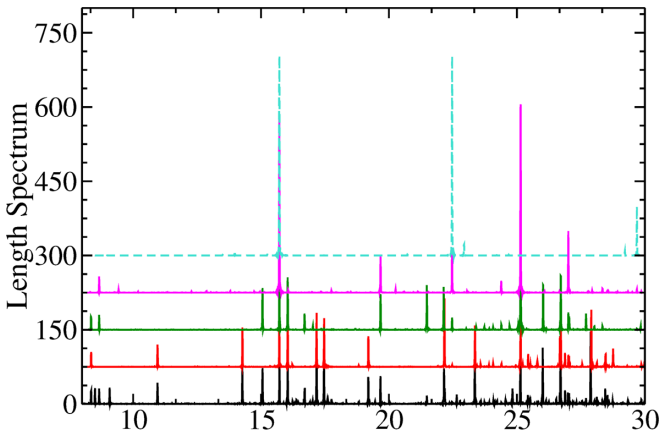

FIG. 11. Length spectra, from bottom to top of the GOE quantum graph with five conventional joints (black line) and of the graphs with one (red), two (green), three (magenta), and four (turquoise) type B joints and conventional type A joints otherwise.

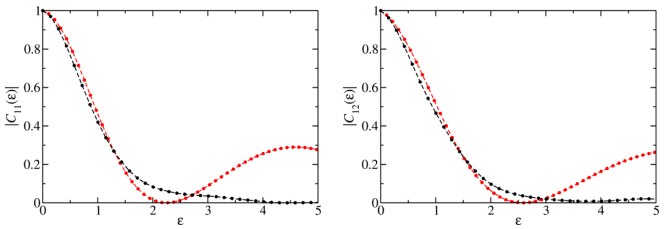

FIG. 12. Autocorrelation functions deduced from the measured reflection (left) and transmission (right) spectra of the unidirectional microwave network (red dots and lines) shown in Fig. 1 in comparison to the RMT result (black dots and lines) for $\tau_{abs} = 2$.

To illustrate the decrease of complexity, i.e., of the number of possible itineraries of waves in networks constructed from an increasing number of vertices governed by Eq. (19), we compare in Fig. 11 length spectra of the graphs with the geometry shown in Fig. 2 with five conventional type A joints (black line), and with one (red), two (green), three (magenta), and four (turquoise) type B joints and conventional type A joints otherwise. It is clearly visible that with increasing number of joints that induce a directionality, the number of periodic orbits decreases considerably, implying that the complexity of the wave dynamics decreases.

IV. FLUCTUATION PROPERTIES OF THE SCATTERING MATRIX

The S-matrix approach [85] used for the derivation of RMT-based analytical results for the fluctuation properties of the S matrix associated with a quantum-chaotic scattering system [23,27,91,93–95] was developed by Mahaux and Weidenmüller in the context of compound nuclear reactions,

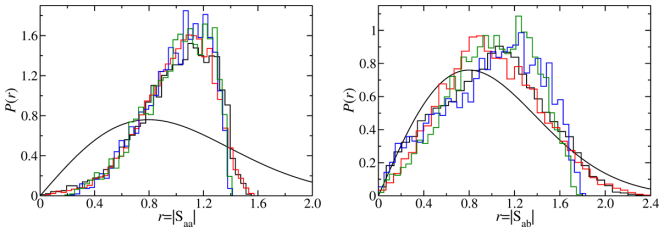

FIG. 13. Left: Distribution of the measured reflection amplitudes $|S_{11}|$ (black) and $|S_{22}|$ (red) of the microwave network shown in Fig. 1 compared to those obtained for the corresponding quantum graph shown in Fig. 2 (green and blue lines, respectively). Right: Same for the transmission spectra $|S_{12}|$ and $|S_{21}|$. The solid black line shows the bivariate Gaussian distribution expected for perfect coupling to the continuum in the Ericson region of strongly overlapping resonances.

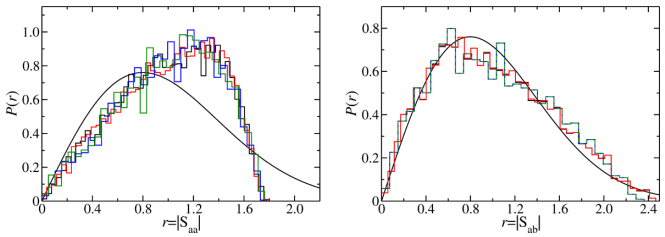

FIG. 14. Left: Distribution of the measured reflection amplitudes $|S_{11}|$ (black) and $|S_{22}|$ (red) of the microwave network shown in Fig. 1 with no isolators compared to those obtained for the corresponding quantum graph shown in Fig. 2 (green and blue lines, respectively). Right: Same for the transmission spectra $|S_{12}|$ and $|S_{21}|$. The solid black line shows the bivariate Gaussian distribution expected for perfect coupling to the continuum in the Ericson region of strongly overlapping resonances.

yielding

$$\hat{S}(k)_{ba} = \delta_{ba} - 2\pi i \sum_{\mu,\nu=1}^{N} \hat{W}^{*}_{\mu b}[(k\mathbb{1} - \hat{H}^{\text{eff}})^{-1}]_{\mu\nu}\hat{W}_{\nu a}. \quad (27)$$

We apply it to microwave networks and open quantum graphs. In a microwave network a and b refer to the antenna channels and $\hat{H}^{\text{eff}} = \hat{H} - i\pi\hat{W}\hat{W}^{\dagger}$ with $\hat{H}$ referring to the k-independent RMT Hamiltonian and $(k\mathbb{1} - \hat{H})$ simulating the spectral fluctuation properties of the closed quantum graph, i.e., of $\hat{h}(k)$ in Eq. (6). For a quantum graph with preserved or violated $\mathcal{T}$ invariance $\hat{H}$ is replaced by a random $(N \times N)$-dimensional matrix from the GOE or GUE, respectively. The matrix elements $W_{\mu a}$ and $W_{\mu b}$, $\mu = 1, \ldots, N$, describe the coupling of the antenna modes to the microwave networks or of the leads to the quantum graph and may be chosen as real Gaussian distributed numbers [105,106]. Absorption at the joints or in the coaxial cables is modeled [91,93] by Λ fictitious channels $W_{\mu c}$. Since the frequency-averaged S-matrix was diagonal in all microwave network realizations, $\langle S_{ba}\rangle = \langle S_{aa}\rangle\delta_{ba}$, direct processes are negligible. This property is accounted for in the RMT model through the orthogonality property $\sum_{\mu=1}^{N} W_{\mu c}W_{\mu c'} = N w_c^2 \delta_{cc'}$. The eigenvectors of a real symmetric random matrix from the GOE fulfill these properties. Accordingly we chose Λ of them as column vectors of $\hat{W}$. The quantities w_i are the input parameters of the RMT model in Eq. (27) through the transmission coefficients

$$T_c = 1 - |\langle S_{cc}\rangle|^2, \quad (28)$$

which provide a measure for the unitarity deficit of the average S matrix $\langle S\rangle$ and are related to w_c^2 via $T_c = \frac{4\pi^2 w_c^2/d}{(1+\pi^2 w_c^2/d)^2}$ with $d = \sqrt{\frac{2}{N}\langle H_{\mu\mu}^2\rangle}\frac{\pi}{N}$ denoting the mean resonance spacing.

The transmission coefficients T_a and T_b associated with antennas a and b are determined from the measured reflection spectra yielding with Eq. (28) $T_{a,b} \simeq 0.95$ for all measurements, whereas those related to the fictitious channels accounted for through the parameter $\tau_{\text{abs}} = \Lambda T_c$ [93] are determined by fitting analytical results for the two-point correlation function of the S-matrix elements,

$$C_{ab}(\epsilon) = \langle S_{ab}(f)\, S_{ab}^{*}(f+\epsilon)\rangle - |\langle S_{ab}(f)\rangle|^2, \quad (29)$$

to the corresponding experimentally determined ones. These are derived in Refs. [23,27] for the GOE and GUE, respectively, and for the case of partial $\mathcal{T}$ violation in Ref. [93]. We performed for the unidirectional microwave network measurements of the transmission and reflection spectra with isolators added to the ports, which allow only one direction of wave propagation, and without them, yielding the S matrix for a superposition of the two possible directions of propagation. A fit to the associated two-point correlation functions yielded for both cases $\tau_{\text{abs}} = 2$, whereas for the microwave network with one type B joint best agreement between the experimental and RMT results was achieved for $\tau_{\text{abs}} = 4$. When increasing the

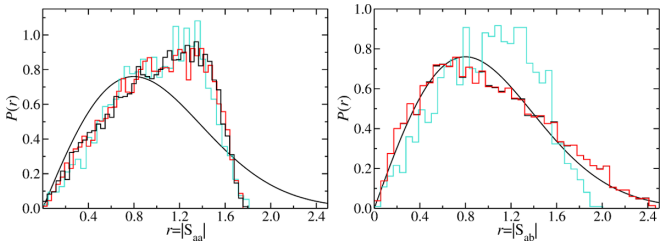

FIG. 15. Left: Distribution of the measured reflection amplitudes $|S_{11}|$ (black) and $|S_{22}|$ (red) of the microwave network shown in Fig. 1 with no isolators compared to those obtained from the RMT model in Eq. (27) with $\tau_{\text{abs}} = 2$ (turquoise line). Right: Same for the transmission spectra $|S_{12}|$ and $|S_{21}|$. The solid black line shows the bivariate Gaussian distribution expected for perfect coupling to the continuum in the Ericson region of strongly overlapping resonances.

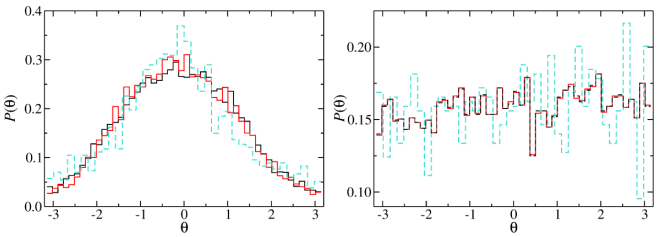

FIG. 16. Same as Fig. 15 for the phases of the S-matrix elements.

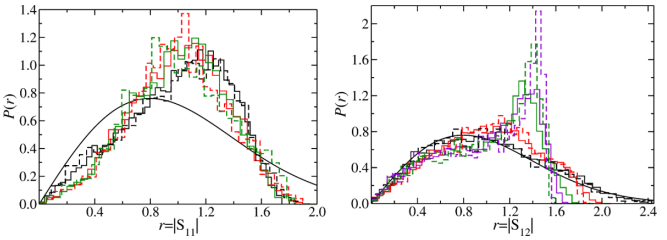

FIG. 17. Left: Distribution of the measured reflection amplitudes $|S_{11}|$ of a microwave network with the same geometry as schematically shown in Fig. 2 with one (black), four (red), and five (green) type B joints and the remainder from conventional type A joints. The dashed lines show the numerical results for the corresponding graphs. Right: Same for the transmission spectra $|S_{12}|$. For the case with four type B joints we also show $|S_{21}|$ (violet), because it differs from $|S_{12}|$ whereas in the other cases the transmission spectra are similar. The solid black line shows the bivariate Gaussian distribution expected for perfect coupling to the continuum in the Ericson region of strongly overlapping resonances.

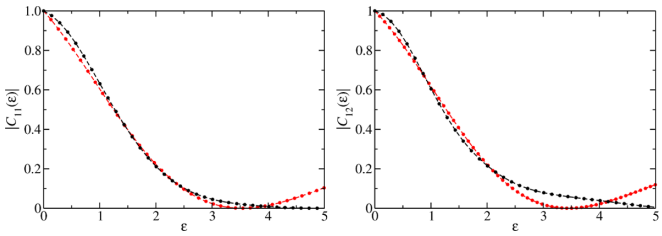

FIG. 18. Autocorrelation functions deduced from the measured reflection (left) and transmission (right) spectra of the GUE microwave network (red) with the geometry shown in Fig. 2 with four conventional type A joints and one type B joint in comparison to the RMT result for $\tau_{\mathrm{abs}} = 4$.

number of type B joints, agreement with RMT predictions becomes worse. The autocorrelation functions obtained from the experimental data (red) are compared in Fig. 12 for the unidirectional microwave network to the corresponding RMT results. In order to verify the experimental results we also computed the S matrix numerically based on Eq. (12) and compared the results of its fluctuation properties to those obtained from the experimental data. To get a good description we had to take into account the absorption present in microwave networks. For this it was sufficient to add a small imaginary part to the wavenumber k in Eq. (14), thus yielding a subunitary bond scattering matrix.

In Fig. 13 we compare the results obtained for the reflection-scattering (left) and transmission-scattering (right) amplitudes for the unidirectional quantum graphs admitting only one direction of wave propagation, respectively, to those obtained with the microwave network shown in Fig. 1. We attribute small deviations observed in the right panel for large values of the transmission-scattering amplitudes to the effect of the isolators which cannot fully avoid wave propagation in the other direction. In Fig. 14 we compare the results obtained for the reflection-scattering (left) and transmission-scattering (right) amplitudes for the unidirectional quantum graph admitting both directions of wave propagation to those obtained with the microwave network shown in Fig. 1 after removal

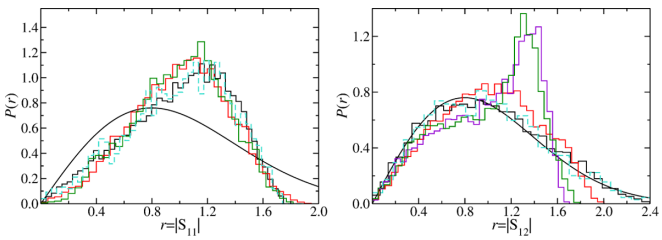

FIG. 19. Left: Distribution of the measured reflection amplitudes $|S_{11}|$ of a microwave network with the same geometry as schematically shown in Fig. 2 with one (black), four (red), and five (green) type B joints and type A joints otherwise. The dashed turquoise lines show the RMT results for $\tau_{\mathrm{abs}} = 4$. Right: Same for the transmission spectra $|S_{12}|$. For the case with four type B joints we also show $|S_{21}|$ (violet), because it differs from $|S_{12}|$ whereas in the other cases the transmission spectra are similar. The solid black line shows the bivariate Gaussian distribution expected for perfect coupling to the continuum in the Ericson region of strongly overlapping resonances.

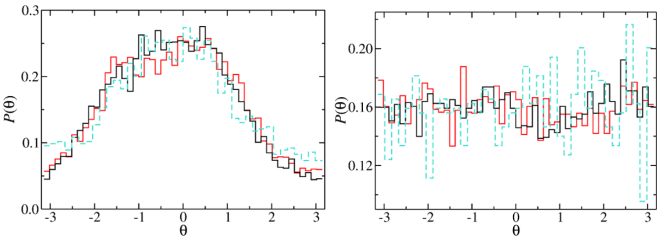

FIG. 20. Same as Fig. 19 for the phases of the S-matrix elements for the case with four conventional type A joints and one type B joint.

of the isolators ISO 01 and ISO 02. Agreement between the numerical and experimental results is good after adding a small imaginary part to the wavenumber which has the same size as in the case where only one direction of propagation is possible. We may conclude that this modeling of absorption is appropriate. In Figs. 15 and 16 we compare the distributions for the modulus and phase of the diagonal (left) and off-diagonal (right) S-matrix elements with the RMT results for the GUE where we used the values of the transmission coefficients and of τ_{abs} obtained from Eq. (28) and the fit to the correlation functions in Eq. (29). Agreement is best for the distribution of the modulus of the diagonal elements, whereas clear deviations are observed for the off-diagonal elements. Other choices of the values for $T_{1,2}$ and τ_{abs} yielded similar deviations. For the case with isolators, that is, with one allowed direction of propagation, we did not find any agreement with RMT results for the GUE. We conclude that the fluctuation properties of the S matrix associated with open unidirectional quantum graphs do not follow RMT predictions for typical quantum chaotic scattering systems. In order to demonstrate that these deviations are due to the unidirectionality, that is, they may be attributed to a loss of complexity due to the associated restrictions on the possible directions of wave propagation in the graphs (respectively networks), we investigated the fluctuation properties of open graphs with the geometry in Fig. 2, constructed from conventional type A and type B joints governed by Eqs. (10) and (19), respectively. In Fig. 17 we compare the distributions of the modulus of the diagonal (left) and off-diagonal (right) S-matrix elements for one (black), four (red), and five (green) type B joints, obtained from the experimental (solid lines) and numerical data (dashed lines). We find best agreement with RMT predictions for the GUE graph, that is, for the case with four conventional type A joints and one type B joint. The good agreement between the experimental and numerical distributions demonstrates that the numerical graphs provide a good description of the corresponding microwave network. Results for the correlation functions and the distributions of modulus and phase of the diagonal and off-diagonal S-matrix elements are shown in Figs. 18–20.

V. CONCLUSIONS

We analyze both experimentally and numerically the fluctuation properties in the eigenfrequency spectra and of the S matrix of closed and open unidirectional quantum graphs and compare them to those of conventional GUE graphs of the same geometry. Both types of graphs were constructed from

vertices of valency four, as illustrated in Fig. 2 for the unidirectional one. Unidirectionality is experimentally achieved with hybrids that are described by the vertex matrix given in Eq. (21) whereas microwave networks modeling conventional GUE quantum graphs are constructed from one pair of coupled circulators governed by Eq. (19) and conventional joints characterized by Eq. (10) otherwise. We demonstrate that conventional closed and open GUE graphs exhibit the spectral properties and fluctuations of the S matrix expected for typical chaotic systems with violated time-reversal invariance, except for deviations in the long-range correlations visible, e.g., for the number variance for level distances larger than $L = 3$–4 mean spacings. With increasing number of type B joints and for the unidirectional graph, for which all joints need to be replaced by type C vertices, deviations of the same size as for the conventional GUE graphs are observed in the long-range spectral properties, however, already at distances of $L \approx 1.5$ mean spacings. The short-range correlations of the unidirectional and the GUE graph and of the graphs with less than four type B joints agree well with those of random matrices from the GUE. Yet, the distributions of the S-matrix elements of the corresponding open unidirectional graph and graphs with four type B joints clearly deviate from those of a typical quantum chaotic scattering system. We attribute these observations to the constraints arising from the required directionality and unidirectionality, respectively, which lead to a restriction of the number of possible itineraries through the graph and thus to a loss of complexity of the wave dynamics of the quantum graph. Note that in Ref. [49] GUE graphs were modeled experimentally by attaching a circulator to each conventional joint, so that directionality was imposed only at a part of the bonds attached to them. Still, contributions due to backscattering at vertices were negligible as compared to the impact of missing levels on the spectral properties. Indeed, perfect agreement with missing level statistics was found. We constructed the conventional GUE graph with one type B joint such that the graphs obtained from it by increasing the number of directional vertices simulate the situation of unidirectional graphs as closely as possible in order to corroborate our supposition that deviations from GUE statistics observed in the long-range correlations of unidirectional quantum graphs may be attributed to a loss of complexity. Note that Ref. [69] focuses on short-range correlations, and analytical results are derived for the nearest-neighbor spacing distributions that were shown to provide a very good description for unidirectional and nearly unidirectional quantum graphs. We also find good agreement for the short-range correlations and deviations in the long-range correlations for distances larger than $L \approx 1.5$ mean spacings, so that our findings are not contradictory to theirs.

ACKNOWLEDGMENTS

This work was supported by the National Natural Science Foundation of China under Grants No. 11775100, No. 11961131009, and No. 12047501. B.D. and W.Z. acknowledge financial support from the Institute for Basic Science in Korea through the Project No. IBS-R024-D1. B.D. thanks Uzy Smilansky for fruitful discussions and his constructive advice.

[1] T. Kottos and U. Smilansky, Phys. Rev. Lett. **79**, 4794 (1997).
[2] T. Kottos and U. Smilansky, Ann. Phys. **274**, 76 (1999).
[3] P. Pakonski, K. Zyczkowski, and M. Kus, J. Phys. A: Math. Gen. **34**, 9303 (2001).
[4] C. Texier and G. Montambaux, J. Phys. A: Math. Gen. **34**, 10307 (2001).
[5] P. Kuchment, Waves Random Media **14**, S107 (2004).
[6] S. Gnutzmann and U. Smilansky, Adv. Phys. **55**, 527 (2006).
[7] G. Berkolaiko and P. Kuchment, *Introduction to Quantum Graphs* (American Mathematical Society, Providence, RI, 2013).
[8] L. Pauling, J. Chem. Phys. **4**, 673 (1936).
[9] J. A. Sánchez-Gil, V. Freilikher, I. Yurkevich, and A. A. Maradudin, Phys. Rev. Lett. **80**, 948 (1998).
[10] V. Kostrykin and R. Schrader, J. Phys. A: Math. Gen. **32**, 595 (1999).
[11] S. W. L. R. Mittra, *Analytical Techniques in the Theory of Guided Waves* (Macmillan, New York, 1971).
[12] D. Kowal, U. Sivan, O. Entin-Wohlman, and Y. Imry, Phys. Rev. B **42**, 9009 (1990).
[13] Y. Imry, *Introduction to Mesoscopic Systems* (Oxford University Press, Oxford, UK, 1996).
[14] J. M. Harrison, U. Smilansky, and B. Winn, J. Phys. A: Math. Theor. **40**, 14181 (2007).
[15] M. Ławniczak, J. Lipovský, and L. Sirko, Phys. Rev. Lett. **122**, 140503 (2019).
[16] S. Gnutzmann and A. Altland, Phys. Rev. Lett. **93**, 194101 (2004).
[17] M. L. Mehta, *Random Matrices* (Academic Press, London, 1990).
[18] O. Bohigas, M. J. Giannoni, and C. Schmit, Phys. Rev. Lett. **52**, 1 (1984).
[19] T. Guhr, A. Müller-Groeling, and H. A. Weidenmüller, Phys. Rep. **299**, 189 (1998).
[20] F. Haake, S. Gnutzmann, and M. Kuś, *Quantum Signatures of Chaos* (Springer-Verlag, Heidelberg, 2018).
[21] S. Heusler, S. Müller, A. Altland, P. Braun, and F. Haake, Phys. Rev. Lett. **98**, 044103 (2007).
[22] J. Keating, Nonlinearity **4**, 309 (1991).
[23] J. Verbaarschot, H. Weidenmüller, and M. Zirnbauer, Phys. Rep. **129**, 367 (1985).
[24] Z. Pluhař and H. A. Weidenmüller, Phys. Rev. Lett. **110**, 034101 (2013).
[25] Z. Pluhař and H. A. Weidenmüller, Phys. Rev. E **88**, 022902 (2013).
[26] Z. Pluhař and H. A. Weidenmüller, Phys. Rev. Lett. **112**, 144102 (2014).
[27] Y. V. Fyodorov, D. V. Savin, and H.-J. Sommers, J. Phys. A: Math. Gen. **38**, 10731 (2005).
[28] H. I. Liou, H. S. Camarda, and F. Rahn, Phys. Rev. C **5**, 1002 (1972).
[29] T. Zimmermann, H. Köppel, L. S. Cederbaum, G. Persch, and W. Demtröder, Phys. Rev. Lett. **61**, 3 (1988).

[30] T. Guhr and H. A. Weidenmüller, Ann. Phys. **193**, 472 (1989).
[31] H. A. Weidenmüller and G. E. Mitchell, Rev. Mod. Phys. **81**, 539 (2009).
[32] J. Gómez, K. Kar, V. Kota, R. Molina, A. Relaño, and J. Retamosa, Phys. Rep. **499**, 103 (2011).
[33] A. Frisch, M. Mark, K. Aikawa, F. Ferlaino, J. L. Bohn, C. Makrides, A. Petrov, and S. Kotochigova, Nature (London) **507**, 475 (2014).
[34] J. Mur-Petit and R. A. Molina, Phys. Rev. E **92**, 042906 (2015).
[35] B. Dietz, A. Heusler, K. H. Maier, A. Richter, and B. A. Brown, Phys. Rev. Lett. **118**, 012501 (2017).
[36] P. Naubereit, D. Studer, A. V. Viatkina, A. Buchleitner, B. Dietz, V. V. Flambaum, and K. Wendt, Phys. Rev. A **98**, 022506 (2018).
[37] *Chaos and Quantum Physics*, edited by M. Giannoni, A. Voros, and J. Zinn-Justin (Elsevier, Amsterdam, 1989).
[38] H.-J. Stöckmann, *Quantum Chaos: An Introduction* (Cambridge University Press, Cambridge, UK, 2000).
[39] S. Sridhar, Phys. Rev. Lett. **67**, 785 (1991).
[40] H.-D. Gräf, H. L. Harney, H. Lengeler, C. H. Lewenkopf, C. Rangacharyulu, A. Richter, P. Schardt, and H. A. Weidenmüller, Phys. Rev. Lett. **69**, 1296 (1992).
[41] J. Stein and H.-J. Stöckmann, Phys. Rev. Lett. **68**, 2867 (1992).
[42] P. So, S. M. Anlage, E. Ott, and R. N. Oerter, Phys. Rev. Lett. **74**, 2662 (1995).
[43] S. Deus, P. M. Koch, and L. Sirko, Phys. Rev. E **52**, 1146 (1995).
[44] H.-J. Stöckmann, M. Barth, U. Dörr, U. Kuhl, and H. Schanze, Physica E **9**, 571 (2001).
[45] B. Dietz and A. Richter, Chaos **25**, 097601 (2015).
[46] O. Hul, S. Bauch, P. Pakoński, N. Savytskyy, K. Życzkowski, and L. Sirko, Phys. Rev. E **69**, 056205 (2004).
[47] C. Dembowski, B. Dietz, H.-D. Gräf, A. Heine, T. Papenbrock, A. Richter, and C. Richter, Phys. Rev. Lett. **89**, 064101 (2002).
[48] M. Ławniczak, S. Bauch, O. Hul, and L. Sirko, Phys. Rev. E **81**, 046204 (2010).
[49] M. Białous, V. Yunko, S. Bauch, M. Ławniczak, B. Dietz, and L. Sirko, Phys. Rev. Lett. **117**, 144101 (2016).
[50] A. Rehemanjiang, M. Allgaier, C. H. Joyner, S. Müller, M. Sieber, U. Kuhl, and H.-J. Stöckmann, Phys. Rev. Lett. **117**, 064101 (2016).
[51] A. M. Martínez-Argüello, A. Rehemanjiang, M. Martínez-Mares, J. A. Méndez-Bermúdez, H.-J. Stöckmann, and U. Kuhl, Phys. Rev. B **98**, 075311 (2018).
[52] A. M. Martínez-Argüello, J. A. Méndez-Bermúdez, and M. Martínez-Mares, Phys. Rev. E **99**, 062202 (2019).
[53] J. Lu, J. Che, X. Zhang, and B. Dietz, Phys. Rev. E **102**, 022309 (2020).
[54] J. Che, J. Lu, X. Zhang, B. Dietz, and G. Chai, Phys. Rev. E **103**, 042212 (2021).
[55] M. Ławniczak, O. Hul, S. Bauch, P. Seba, and L. Sirko, Phys. Rev. E **77**, 056210 (2008).
[56] M. Ławniczak, S. Bauch, O. Hul, and L. Sirko, Phys. Scr. T **143**, 014014 (2011).
[57] O. Hul, M. Ławniczak, S. Bauch, A. Sawicki, M. Kuś, and L. Sirko, Phys. Rev. Lett. **109**, 040402 (2012).
[58] M. Ławniczak, A. Sawicki, S. Bauch, M. Kuś, and L. Sirko, Phys. Rev. E **89**, 032911 (2014).
[59] M. Ławniczak, B. van Tiggelen, and L. Sirko, Phys. Rev. E **102**, 052214 (2020).
[60] M. Robnik and M. V. Berry, J. Phys. A: Math. Gen. **19**, 669 (1986).
[61] J. M. Robbins, Phys. Rev. A **40**, 2128 (1989).
[62] F. Leyvraz, C. Schmit, and T. H. Seligman, J. Phys. A: Math. Gen. **29**, L575 (1996).
[63] C. H. Joyner, S. Müller, and M. Sieber, J. Phys. A: Math. Theor. **45**, 205102 (2012).
[64] W. Zhang and B. Dietz, Phys. Rev. B **104**, 064310 (2021).
[65] B. Gutkin, J. Phys. A: Math. Theor. **40**, F761 (2007).
[66] G. Veble, T. Prosen, and M. Robnik, New J. Phys. **9**, 15 (2007).
[67] B. Gutkin, Proc. Am. Math. Soc. **137**, 2795 (2009).
[68] B. Dietz, T. Guhr, B. Gutkin, M. Miski-Oglu, and A. Richter, Phys. Rev. E **90**, 022903 (2014).
[69] M. Akila and B. Gutkin, J. Phys. A: Math. Theor. **48**, 345101 (2015).
[70] S. Gnutzmann, H. Schanz, and U. Smilansky, Phys. Rev. Lett. **110**, 094101 (2013).
[71] B. Dietz, V. Yunko, M. Białous, S. Bauch, M. Ławniczak, and L. Sirko, Phys. Rev. E **95**, 052202 (2017).
[72] M. Sieber, U. Smilansky, S. C. Creagh, and R. G. Littlejohn, J. Phys. A: Math. Gen. **26**, 6217 (1993).
[73] P. Exner and M. Tater, Phys. Lett. A **382**, 283 (2018).
[74] J. Yusupov, K. Sabirov, M. Ehrhardt, and D. Matrasulov, Phys. Lett. A **383**, 2382 (2019).
[75] M. V. Berry, Proc. R. Soc. London A **400**, 229 (1985).
[76] A. Relaño, J. M. G. Gómez, R. A. Molina, J. Retamosa, and E. Faleiro, Phys. Rev. Lett. **89**, 244102 (2002).
[77] E. Faleiro, J. M. G. Gómez, R. A. Molina, L. Muñoz, A. Relaño, and J. Retamosa, Phys. Rev. Lett. **93**, 244101 (2004).
[78] R. Molina, J. Retamosa, L. Muñoz, A. Relaño, and E. Faleiro, Phys. Lett. B **644**, 25 (2007).
[79] J. Che, B. Dietz, G. Chai, and H. Teng, Owner Lanzhou University, Radio Frequency Adapter (2021). Patent No. ZL 2021 2 1328920.8.
[80] D. S. Jones, *Theory of Electromagnetism* (Pergamon, New York, 1964).
[81] N. Savytskyy, A. Kohler, S. Bauch, R. Blümel, and L. Sirko, Phys. Rev. E **64**, 036211 (2001).
[82] T. Kottos and U. Smilansky, J. Phys. A: Math. Gen. **36**, 3501 (2003).
[83] H.-J. Stöckmann and J. Stein, Phys. Rev. Lett. **64**, 2215 (1990).
[84] B. Dietz, T. Klaus, M. Miski-Oglu, and A. Richter, Phys. Rev. B **91**, 035411 (2015).
[85] C. Mahaux and H. A. Weidenmüller, *Shell Model Approach to Nuclear Reactions* (North Holland, Amsterdam, 1969).
[86] S. Albeverio, F. Haake, P. Kurasov, M. Kuś, and P. Šeba, J. Math. Phys. **37**, 4888 (1996).
[87] E. Doron, U. Smilansky, and A. Frenkel, Phys. Rev. Lett. **65**, 3072 (1990).
[88] R. A. Méndez-Sánchez, U. Kuhl, M. Barth, C. H. Lewenkopf, and H.-J. Stöckmann, Phys. Rev. Lett. **91**, 174102 (2003).
[89] U. Kuhl, M. Martínez-Mares, R. A. Méndez-Sánchez, and H.-J. Stöckmann, Phys. Rev. Lett. **94**, 144101 (2005).
[90] B. Dietz, T. Friedrich, H. L. Harney, M. Miski-Oglu, A. Richter, F. Schäfer, and H. A. Weidenmüller, Phys. Rev. E **78**, 055204(R) (2008).
[91] B. Dietz, T. Friedrich, H. L. Harney, M. Miski-Oglu, A.

Richter, F. Schäfer, and H. A. Weidenmüller, Phys. Rev. E **81**, 036205 (2010).
[92] B. Dietz, H. Harney, A. Richter, F. Schäfer, and H. Weidenmüller, Phys. Lett. B **685**, 263 (2010).
[93] B. Dietz, T. Friedrich, H. L. Harney, M. Miski-Oglu, A. Richter, F. Schäfer, J. Verbaarschot, and H. A. Weidenmüller, Phys. Rev. Lett. **103**, 064101 (2009).
[94] S. Kumar, A. Nock, H.-J. Sommers, T. Guhr, B. Dietz, M. Miski-Oglu, A. Richter, and F. Schäfer, Phys. Rev. Lett. **111**, 030403 (2013).
[95] S. Kumar, B. Dietz, T. Guhr, and A. Richter, Phys. Rev. Lett. **119**, 244102 (2017).
[96] V. Oganesyan and D. A. Huse, Phys. Rev. B **75**, 155111 (2007).
[97] Y. Y. Atas, E. Bogomolny, O. Giraud, and G. Roux, Phys. Rev. Lett. **110**, 084101 (2013).
[98] Y. Atas, E. Bogomolny, O. Giraud, P. Vivo, and E. Vivo, J. Phys. A: Math. Theor. **46**, 355204 (2013).
[99] J. M. G. Gómez, A. Relaño, J. Retamosa, E. Faleiro, L. Salasnich, M. Vraničar, and M. Robnik, Phys. Rev. Lett. **94**, 084101 (2005).
[100] L. Salasnich, Phys. Rev. E **71**, 047202 (2005).
[101] M. S. Santhanam and J. N. Bandyopadhyay, Phys. Rev. Lett. **95**, 114101 (2005).
[102] A. Relaño, Phys. Rev. Lett. **100**, 224101 (2008).
[103] E. Faleiro, U. Kuhl, R. Molina, L. Muñoz, A. Relaño, and J. Retamosa, Phys. Lett. A **358**, 251 (2006).
[104] O. Bohigas and M. P. Pato, Phys. Lett. B **595**, 171 (2004).
[105] B. Dietz, A. Heine, A. Richter, O. Bohigas, and P. Leboeuf, Phys. Rev. E **73**, 035201(R) (2006).
[106] B. Dietz, T. Friedrich, H. L. Harney, M. Miski-Oglu, A. Richter, F. Schäfer, and H. A. Weidenmüller, Phys. Rev. Lett. **98**, 074103 (2007).